Atmos. Chem. Phys. Discuss., 10, 9077–9120, 2010
www.atmos-chem-phys-discuss.net/10/9077/2010/

Atmospheric Chemistry and Physics Discussions

This discussion paper is/has been under review for the journal Atmospheric Chemistry and Physics (ACP). Please refer to the corresponding final paper in ACP if available.

The relative importance of various source regions on East Asian surface ozone

T. Nagashima[1], **T. Ohara**[1], **K. Sudo**[2,3], **and H. Akimoto**[4]

[1]Asian Environment Research Group, National Institute for Environmental Studies, Tsukuba, Japan
[2]Graduate School of Environmental Studies, Nagoya University, Nagoya, Japan
[3]Research Institute for Global Change, Japan Agency for Marine-Earth Science and Technology, Yokohama, Japan
[4]Acid Deposition and Oxidant Research Center, Niigata, Japan

Received: 4 March 2010 – Accepted: 26 March 2010 – Published: 9 April 2010

Correspondence to: T. Nagashima (nagashima.tatsuya@nies.go.jp)

Published by Copernicus Publications on behalf of the European Geosciences Union.

Abstract

The Source-Receptor (S-R) relationship for surface O_3 in East Asia is estimated for recent years in this study utilizing the tagged tracer method with a global chemical transport model. The estimation shows the importance of intra-continental transport of O_3 inside East Asia as well as the transport of O_3 from distant source regions. The model well simulated the absolute concentration and seasonal variation of surface O_3 in the East Asian region, and demonstrated significant seasonal difference in the origin of surface O_3. More than half of surface O_3 is attributable to the O_3 transported from distant sources outside of East Asia in the cold season (October to March). In the warm season (April to September), most of the surface O_3 is attributed to O_3 created within East Asia in most areas of East Asia. The contribution of domestically-created O_3 accounts for 20% of surface O_3 in Japan and the Korean Peninsula, 40% in North China Plain and around 50% in the southern part of China in spring, which increase greatly in summer. The contribution of China and the Korean Peninsula to Japan are estimated at about 10% and 5%, respectively. A large contribution (20%) of China to the Korean Peninsula is also demonstrated. In the northern and southern part of China, large contribution of over 10% from East Siberia and the Indochina Peninsula are identified, respectively. The contribution of intercontinental transport increases with latitude; it is 21% in Northeast China and 13% in Japan and the Korean Peninsula in spring. As for one-hourly mean surface O_3, domestically-created O_3 is the main contributor in most areas of East Asia, except for the low O_3 class (<30 ppbv), and accounts for more than 50% in very high O_3 class (>90 ppbv). The mean relative contribution of China to central Japan was about 10% in every class, but that from the Korean Peninsula is important in all expect the low O_3 class. Substantial impact of foreign sources on the exceedance of Japan's AAQS is identified in the high O_3 class (60–90 ppbv) in spring.

ACPD

10, 9077–9120, 2010

1 Introduction

Tropospheric ozone (O_3) near the Earth's surface can be a harmful atmospheric pollutant, since high levels of O_3 can have detrimental effects on human health (US Environmental Protection Agency – US EPA, 2006) and cause biochemical damages to plants reducing plant primary productivity and crop yields (Lesser et al., 1990; Kobayashi, 1999; Wang et al., 2005; US EPA, 2006). It is now well established that the concentration of surface O_3 in a given region is controlled through a balance between transport from outside of the region including other continents and the stratosphere, dry deposition onto the surface, and photochemical reactions involving nitrogen oxides (NO_x=NO+NO_2), carbon monoxide (CO), and Volatile Organic Carbons (VOC) on a local and regional scale (Brasseur et al., 1999; Stevenson et al., 2006; Wild, 2007). Intense emissions of these precursors of O_3 (NO_x, CO, and VOCs) from industrial activities, electrical power generation and road transportation cause photochemical smog around big cities and industrial regions. Japan has experienced severe photochemical smog associated with economic growth and motorization in the early 1970s, which was followed by a remarkable improvement of air quality in the subsequent decade due to enactment and gradual reinforcement of regulations against emissions of O_3 precursors. Since then, concentrations of non-methane hydrocarbons over Japan has been continuously decreasing, and NO_x concentration has remained almost constant during the 1980s and 1990s followed by a decrease after 2000. In spite of this, long-term monitoring data shows that surface concentration of O_3 over Japan began to re-increase in the mid 1980s and has continuously increased until the present (Ohara and Sakata, 2003). This increase in surface O_3 has been observed over almost the whole region of Japan including remote monitoring sites located on mountains or islands where no major source of O_3 precursors exists (Ohara and Sakata, 2003; Tanimoto, 2009). These observed features of air quality in Japan strongly suggest that the recent increase in O_3 can not be solely attributed to local pollution as in the early 1970s but is influenced by the transport of O_3 from outside of Japan.

ACPD
10, 9077–9120, 2010

In other East Asian countries, an increasing trend in O_3 concentration has also been observed in mainland China, Hong Kong, and Taiwan (Chou et al., 2006; Lu and Wang, 2006; Chang and Lee; 2007, Xu et al., 2008; Wang et al., 2009), which implies that the increase in O_3 is an issue for the whole East Asian region. The estimated increase in anthropogenic emissions of O_3 precursors in East Asian countries during the last two decades (Ohara et al., 2007), which is verified by space-based measurement of an increase in tropospheric column NO_2 (Richter et al., 2005; Irie et al., 2005), is likely a major cause of the observed increase in East Asian O_3. However, the influence of O_3 precursors emitted in regions outside of East Asia or the influence of stratospheric O_3 upon the observed increase in East Asian O_3 should not be ruled out, because insufficient knowledge of the relative importance of each source region of O_3 on the amount of O_3 over East Asian region is available. Therefore, before discussing the causes of the recent increase in East Asian O_3, quantitative estimation of the amount of O_3 that is transported into East Asia from outside sources, and also the amount of O_3 transported intra-continentally among the East Asian countries is required.

Such quantitative estimations of the proportion of O_3 over a receptor area that is attributable to a source region, the so-called Source-Receptor (S-R) relationship for O_3, has been widely studied (Wang et al., 1998; Jacob et al., 1999; Wild and Akimoto, 2001; Fiore et al., 2002; Li et al., 2002; Derwent et al., 2004; Wild et al., 2004; Auvray and Bey, 2005; Sudo and Akimoto, 2007). Moreover, the international coordinated effort to quantify and estimate uncertainties in the S-R relationship for O_3 and other air pollutants have been proceeding under the United Nations Economic Commission for Europe (UNECE) Convention in Long Range Transboundary Air Pollution (CLRTAP), the Task Force on Hemispheric Transport of Air Pollution (TF HTAP) (Keating and Zuber, 2007; Fiore et al., 2009). However, many of these studies focus on the intercontinental transport of O_3 between the highly populated and industrialized regions in the mid latitudes of the Northern Hemisphere, i.e., North America, Europe and Asia, and pay little attention to the intra-continental transport of O_3.

ACPD
10, 9077–9120, 2010

There are a small number of studies which address the S-R relationship for O_3 in Asia. For instance, Li et al. (2008) studied source apportionment of O_3 observed at Mt. Tai in central eastern China during a field campaign carried out in June 2006 (Kanaya et al., 2009) using a regional chemical transport model. They estimate contributions from defined source regions, which are closely partitioned within China, to the O_3 amount at Mt. Tai. However, a one-month estimation at one particular receptor point only cannot provide the whole picture of the S-R relationship for O_3 in the East Asian region. The S-R relationship for acidifying species over a longer timeframe has already been estimated for sulfur deposition (Carmichael et al., 2002; Lin et al., 2008), but for O_3, such estimations of the S-R relationship have yet to be reported.

In this study, we estimate the S-R relationship for O_3, in particular for surface O_3, in East Asia based on previous work by Sudo and Akimoto (2007), which have demonstrated the significant role of intercontinental transport of O_3 on the global distributions and budgets of tropospheric O_3 using the tagged tracer method with a global chemical transport model. Our current study further investigates contributions from various source regions to the East Asian O_3 concentrations taking into account intra-continental transport as well as intercontinental transport of O_3. The estimation is made through a multi-year simulation over the early 2000s using global-scale chemical transport model with the tagged tracer method to obtain the averaged picture of S-R relationship for O_3 in recent years. In the next section, a brief description of the model and experimental method are presented. The model simulation is evaluated against observations at surface monitoring sites, and the simulated contributions from various source regions are then discussed in Sect. 3. The difference in estimated contributions depending on the class of one-hourly surface O_3 concentration is also discussed in Sect. 3.

2 Method

Generally, there are two different approaches used to quantify the contributions of source regions of O_3 to the amount of O_3 in a receptor area. One is the emission

ACPD
10, 9077–9120, 2010

sensitivity approach, which performs two simulations: a perturbed run with and a standard run without a perturbation in the O_3 precursor emission, respectively, of the designated source region or source sector, to obtain the contribution of that source to O_3 in a receptor region by taking the difference of calculated O_3 between the two runs (Jacob et al., 1999; Wild and Akimoto, 2001; Wild et al., 2004; Fiore et al., 2009). The second approach is the tagged tracer method, which calculates the distribution of hypothetical O_3 tracers, each of which is allowed to be chemically produced only inside its designated source region. Then, the concentration of each O_3 tracer tagged by its source region represents the contribution of that source region. This method has been used in many studies addressing a wide variety of issues using both global and regional chemistry transport models (Wang et al., 1998; Fiore et al., 2002; Li et al., 2002; Auvray and Bey, 2005; Sudo and Akimoto, 2007; Li et al., 2008).

The emission sensitivity approach estimates the amount of O_3 in a receptor region which is produced by, and is thus attributable to, the precursors of O_3 emitted inside each source region no matter where they were chemically converted to O_3. In contrast, the tagged tracer method calculates the amounts of O_3 in a receptor area which was chemically produced inside each source region and then transported to that receptor area, which inevitably includes amounts of O_3 created inside a source region from precursors emitted in adjacent source regions and transported to that source region. Therefore, the S-R relationships for O_3 estimated by these two different approaches can differ. Li et al. (2008) compared the two methods for the contribution of high O_3 production regions in China to O_3 concentration at Mt. Tai in June 2006 and found the difference can be up to 30%. They concluded that both approaches agree reasonably well with each other. Although this one example does not guarantee consistency between the approaches, we decided to employ the tagged tracer method in this study mainly because of its computational efficiency. This study aims to estimate the mean contributions from many source regions (number of region N>20) separately with multi-year model simulations, which requires N+1 runs to deduce the contribution of each source region for a single year using emission sensitivity approach, whereas

the tagged tracer method requires only two runs for a single year using the framework described in the following section.

2.1 Model description

A chemistry climate model for the troposphere, CHASER (Sudo et al., 2002a), is used in this study. CHASER has been developed based on the atmospheric component of a coupled general circulation model, MIROC, developed by the Center for Climate System Research (CCSR), the National Institute for Environmental Studies (NIES), and the Frontier Research Center for Global Change (FRCGC) (Numaguti et al., 1995; K-1 Model Developers, 2004). The framework of the model is basically identical to that used in previous work by Sudo and Akimoto (2007), hereafter referred to as SA07. However, this study uses a finer horizontal grid spacing (T63: ≈1.9° by 1.9° in longitude and latitude) than previously used (T42: ≈2.8° by 2.8°) in order to better resolve individual Asian countries, since the aim is to investigate intra-continental transport of O_3 as well as intercontinental transport of O_3. The top layer of the model is set at about 40 km altitude with 32 vertical layers. The model calculates the concentrations of 53 chemical species through 27 photolysis and 113 chemical reactions representing a detailed tropospheric chemistry involving the O_3-HO_x-NO_x-CH_4-CO system and oxidation of NMHCs. The model also includes the sulfate formation process with gas and liquid phase oxidation of SO_2 and dimethyl sulfide (DMS). A dry deposition scheme based on the resistance series parameterization of Wesely (1989) and two different processes of wet deposition (in-cloud and below-cloud scavenging) are also included. The advective transport of chemical species is calculated with a fourth-order flux-form advection scheme of the monotonic van Leer (van Leer, 1997) and the flux-form semi-Lagrangian advection scheme of Lin and Rood (1996). Vertical transport by moist convection is also considered in the cumulus convection process, which is based on the Arakawa-Schubert scheme (Emori et al., 2001). The concentrations of O_3 and some nitrogen compounds (NO_x, HNO_3, N_2O_5) above the tropopause are assimilated into the monthly mean output data of a stratospheric chemistry climate model. The

ACPD
10, 9077–9120, 2010

data for the assimilation are taken from Akiyoshi et al. (2009) for O_3, and Takigawa et al. (1999) for the nitrogen compounds.

In this study, two different setups of CHASER are used: full-chemistry setup and tracer-transport setup. The full-chemistry setup calculates the temporal evolution of chemical species through the actual chemical-physical procedure as mentioned above, whereas the tracer-transport setup calculates the temporal evolution of hypothetical O_3 tracers with archived chemical tendencies. The detailed procedure of calculation is described in the next subsection.

2.2 Tracer tagging

The tracer tagging method performed in this study consists of two steps (Sudo and Akimoto, 2007). Firstly, a standard simulation with the full-chemistry setup of CHASER is performed to archive 3-hourly mean 3-D fields of chemical production (P) and loss frequencies (L) of the extended odd oxygen family (O_x=O_3+O+O(^{1}D)+NO_2+2 NO_3+3 N_2O_5+PANs+HNO_3+ other nitrates). We use P and L of the O_x family instead of those of O_3 in order to eliminate the rapid null cycles within the O_x family, as in previous studies (Wang et al., 1998; Li et al., 2002; Fiore et al., 2002). The standard simulation also outputs the daily 3-D distribution and 1-hourly surface concentration of O_3, which are hereafter referred to as "total" O_3. Note that outputted O_3 data is correctly a sum of O_3, O, and O(^{1}D). Since the concentrations of O and O(^{1}D) are both negligible in the troposphere compared to O_3, we refer to the outputted data as O_3 for the sake of clarity. The standard simulation is then followed by the second simulation, which uses the trace-transport setup of CHASER. In the second simulation, the temporal evolution of hypothetical O_3 tracers, each of which is assigned to a particular region in the model domain, are calculated. The assignment of a tracer to each region is done in the following way. The transport and dry deposition of each tracer are calculated in the same way as in the standard simulation, but the chemical evolution of tracers is calculated using the archived P and L of O_x. Each O_3 tracer can

be lost chemically at the frequency of L everywhere in the model domain, but it can be produced chemically only inside its assigned source region. In the stratosphere, the concentration of O_3 tracer assigned to the stratosphere is assimilated into the same stratospheric O_3 data as used in the standard simulation, but those of tracers assigned to the region in the troposphere are all set to zero. In SA07, the O_3 tracer assigned to the stratosphere is assimilated only above 55 hPa altitude in order to avoid the non-negligible contribution of O_3 and precursors transported from the troposphere to the lower stratosphere. However, that procedure is not employed in the present study. Instead, we assimilate the O_3 tracer assigned to the stratosphere over the tropopause defined with the lapse rate; otherwise concentrations of total O_3 in the upper troposphere would be overestimated. The concentration of each O_3 tracer tagged with its assigned source region is then scaled to be the sum of all tagged O_3 tracers, being equal to the total O_3 output by the standard simulation. The resultant concentration of each tagged O_3 tracer at a given location represents the contribution of O_3 that was created in each source region and transported to that location.

For the tracer tagging, we separate the model domain into 45 regions in the stratosphere and 22 regions both in the Planetary Boundary Layer (PBL) and in the Free Troposphere (FT), as shown in Fig. 1. As to the vertical classification between the PBL and FT, SA07 defined the PBL as the six lowermost layers in the model (surface to about 750 hPa) based on the observed and modelled vertical profiles of O_3 production. We adopt the same procedure to separate the PBL from the FT. The same horizontal separation of source regions depicted in Fig. 1 is applied in the PBL and the FT. This horizontal separation is different from that applied in SA07, who employed different horizontal separations for the PBL and the FT, respectively, and most of the oceans and East Siberia were assigned to one source region. In this study, since special focus is put on the intra-continental transport of O_3 inside East Asia, we further separate the source region in East Asia; the Korean Peninsula, the Sea of Japan, and the East China Sea are separately defined. We also set source regions for the North Pacific Ocean and North Atlantic Ocean separately, because our pilot simulation showed that

ACPD
10, 9077–9120, 2010

both regions have non-negligible contributions to East Asian surface O_3, and should be considered independently of each other.

2.3 Experimental design

Model simulations are made for six years from the year 2000 to 2005. The model meteorology (horizontal wind velocities and temperature) is assimilated into the National Center for Environmental Prediction/National Center of Atmospheric Research (NCEP/NCAR) reanalysis 6-hourly data (Kalnay et al., 1996) of the corresponding year. Sea surface temperature and sea ice data to drive the model are taken from Hadley Centre's Sea Ice and Sea Surface Temperature data set (HadISST) (Rayner et al., 1993). For the first step of the full chemistry calculation, we use the following emission data sets of O_3 precursors (NO_x, CO, NMHCs) from various origins. Anthropogenic emission data are from the latest version of the Regional Emission inventory in Asia (REAS ver. 1.2) (Ohara et al., 2007) for the Asian region and the Emission Database for Global Atmospheric Research Version 3.2 (EDGAR3.2) Fast Track 2000 (FT2000) data (Olivier and Berdowski, 2001) for the rest of the world. For O_3 precursor emissions from biomass burning, we adopt vegetation fire emission data compiled for the Reanalysis of the Tropospheric chemical composition over the past 40 years project (RETRO) (Schultz et al., 2008) for the whole land area. We also consider natural sources of NO_x from soils (5.5 TgN/yr) and lightning (3.3 TgN/yr). Large biogenic emissions of isoprene (400 TgC/yr) and terpenes (100 TgC/yr) are used following SA07. The initial condition of the simulation is taken from a 5-year integration using CHASER with constant boundary conditions for the year 2000, which is long enough to obtain the equilibrium state.

ACPD
10, 9077–9120, 2010

3 Results

3.1 Model evaluation with surface ozone observations

The ability of CHASER to represent the observed concentrations of O_3 and related chemical species has been well validated in previous studies (Sudo et al., 2002b; Sudo and Akimoto, 2007). However, we employ a finer horizontal resolution than used in previous studies and the emission data of O_3 precursors and the driving meteorological field have been updated for the current study. Thus, the current model setup of CHASER should be re-validated, particularly against the new observations coincident with the period of model simulation (2000 to 2005).

Figure 2 shows the comparison of annual cycles of modelled monthly mean surface O_3 concentration with observations at 25 selected surface sites whose locations are plotted in Fig. 1. The observations are mainly taken from the database of the World Data Centre for Greenhouse Gasses (WDCGG) (data are available from http://gaw.kishou.go.jp/wdcgg/) and the Acid Deposition Monitoring Network in East Asia (EANET) (data are available from http://www.eanet.cc/product.html). The O_3 data observed at Chinese mountain sites (Mt. Tai, Mt. Hua, and Mt. Huang) by the collaboration between the Frontier Research Center for Global Change (FRCGC) of the Japan Agency for Marine-Earth Science and Technology (JAMSTEC) and the Institute of Atmospheric Physics (IAP) of the Chinese Academy of Science (CAS) were made available for this comparison (Li et al., 2007). For the comparison in the Southeast Asian region, the O_3 data obtained at Srinakarin located in central Thailand are used (Pochanart et al., 2001). The observation sites for the comparison are chosen to cover the wide longitudinal range of Northern Hemisphere mid-latitudes, because the ozone originating from this region has a large impact on the Asian surface O_3 (Wild and Akimoto, 2001; Wild et al., 2004; Sudo and Akimoto, 2007). Only the data observed during the simulation period (2000 to 2005) are compared at each site except at Srinakarin where the two years (1999 and 2000) of available data are used for comparison. In Fig. 2, observed monthly means and range of daily means are shown in coloured circles and

ACPD
10, 9077–9120, 2010

boxes, respectively; red (green) circles and boxes are for observational sites where more than (not exceeding) 2 years of data are available.

Several statistics of comparison depicted in Fig. 2 are summarized in Table 1, which present the annual mean of the observation and model calculation, correlation coefficient (R), Mean Bias (MB), and Root Mean Square Error (RMSE) between the observation and model calculation. In general, the model successfully represents the seasonal cycle of surface O_3 in both polluted and remote regions. The R-values exceed 0.7 at all sites; in particular, those in East Asia on which this study is focussed are generally over 0.8 and even over 0.9 for more than half of the East Asian sites. The values of MB and RMSE show that the absolute concentration of surface O_3 is simulated within a bias of 10 ppbv in most cases. Some details about individual sites are discussed below.

At the remote sites located in inland high-altitude areas (e.g., Zugspitze Schneefernerhause, Niwot Ridge Saddle, Issyk Kul), the broad summer peak of surface O_3 is simulated very well. These summer peaks are mainly attributable to the enhanced contribution of O_3 created in the surrounding region with the leading contribution from the PBL, while the stratospheric contribution has a peak of about 20 ppbv in winter to early spring, which accounts for half of the total O_3 in that time period. At Niwot Ridge Saddle, a bulge during July to August in the observation is well simulated by the model. Von Kuhlmann et al. (2003) reported that a similar bulge could be simulated by their model, but was not seen in the observation with which they compared their model results. The data they used may have been observed at the Niwot Ridge C-1 site, which is located about 5 km east and 500 m lower than the Saddle site. The seasonal cycle of O_3 observed at the C-1 site does not display such a bulge in summer as in the Saddle site data. The available observation of surface O_3 at the Saddle site spans only 15 months from October 2003 to December 2004. Therefore, the bulge may not be a climatological feature, but a specific feature in 2004.

Hohenpeissenberg is located close to Zugspitze and thus shows a distinct broad peak from May to August. The model can simulate this broad summer peak at

ACPD
10, 9077–9120, 2010

Hohenpeissenberg, but the magnitude of the peak is overestimated by 5 to 10 ppbv. This is due to the inability of the model to capture the observed lower portion of daily mean surface O_3 concentration. The observatory at Hohenpeissenberg is surrounded by populated areas typical of Central Western Europe, thus it may suffer from the influence of the NO-titration effect, which can not be resolved at the horizontal resolution of the current model.

The characteristic seasonal cycle with a peak in spring and a trough in summer at the maritime remote sites (Mace Head, Mauna Loa, Heimaey, Trinidad Head, Angra do Heroismo, Tudor Hill, Hedo, Ogaswara) is well simulated by the model. These spring peaks can be understood as a combination of the stratospheric contribution, which peaks from winter to early spring, and the contribution of inter- and intra-continental transport of O_3, which peaks in spring. The winter-spring peak of the stratospheric contribution also can be seen in previous global modelling studies (Roelofs et al., 1997; von Kuhlmann et al., 2003), which show somewhat greater stratospheric contributions than our estimations. The summer trough is associated with the summer monsoon bringing low concentration of O_3 in the marine boundary layer at some East Asian sites (Hedo, Ogasawara, Srinakarin). The stratospheric contribution generally has a minimum in summer at most sites depicted in Fig. 1, but at sites located in the interior of the Eurasian continent (Mondy and Issyk Kul), the minimum of the stratospheric contribution appears in autumn.

3.2 Overview of East Asian surface O_3

Figure 3 illustrates the simulated seasonal mean O_3 concentrations (colours) and wind fields (arrows) at the surface in East Asia and surrounding regions. The belt of most condensed O_3 located between 30° N and 45° N in summer moves southward toward winter, and then returns northward toward summer. This latitudinal movement of the enhanced O_3 belt has also been found in the space-born measurement of tropospheric column O_3 by the Global Ozone Monitoring Experiment (GOME) (Hayashida et al., 2008).

Since the intensity of ultraviolet radiation peaks in summer and thus the chemical production of O_3 also peaks in summer, the surface O_3 over the continental polluted region shows a maximum in summer. On the other hand, as the North Pacific high pressure system intensifies and expands westward in summer, the clean unpolluted maritime air mass, which contains less O_3, is transported around the rim of the North Pacific High and makes south-westerly flow into the East Asia. The competition between the influence of these continental and maritime air masses results in several types of seasonal cycles of surface O_3 in East Asian countries. In two of the mountain sites in China (Mt. Tai and Mt. Hua) depicted in Fig. 2, the peak occurs in June followed by a small trough in summer, which shows that the two sites are strongly influenced by continental air but a small influence of maritime air in summer is also discernible. However, at another mountain site in China (Mt. Huang), which is located at more southward and closer to the ocean, the seasonal cycle of surface O_3 displays a distinct summer minimum. These features of seasonal variation observed at the three mountain sites in China are well simulated by the model.

The similar distinct summer minimum observed at Mt. Huang can also be seen in the observations at Japanese and South Korean sites (Rishiri, Ryori, Oki, Happo, Hedo, Kanghwa, and Cheju), since both countries lie at the boundary region between continental and maritime air masses. The surface O_3 at these sites have a peak in spring followed by a trough in summer and a second peak in autumn. The model results at these sites show similar seasonal variation as observed, but the magnitude of the summer trough is generally underestimated; thus the concentrations of O_3 at some of these sites (e.g., Ryori, Oki, Kanghwa, and Cheju) are overestimated in summer. A similar tendency to overestimate summertime O_3 around Japan can be seen in other global model studies (Fiore et al., 2009). Fiore et al. (2009) notices that the insufficient representation of clean air in the North Pacific High in the model is one possible cause, but the cause of the insufficient decline of summertime O_3 in our model is still not clear.

At the Japanese mountainous site (Happo), there is year-round underestimation of O_3 by the model. The modelled range of daily mean surface O_3 at Happo is apparently

ACPD
10, 9077–9120, 2010

biased towards lower concentration of O_3 compared to the observation, which means that the model can not well represent the occurrence of high-O_3 days. The occurrence of such high concentration of O_3 might be influenced by polluted air from surrounding cities coupled with the detailed terrain structure and meteorology in the mountainous area, which can not be resolved by the coarse horizontal resolution of the current model.

At the site located in the northern part of Japan (Rishiri), the model underestimates the surface O_3 in winter and spring by about 10 to 15 ppbv. Since the O_3 transported from distant regions contributes significantly in the northern part of Japan in winter to early spring as shown later, these long range transported O_3 might be underestimated. We introduced the reduction of dry deposition at a lower temperature that is described in the original literature of the parameterization of dry deposition by Wesely (1989) in order to reduce the underestimation of surface O_3 in the northern part of Japan. This may have partly eliminated the underestimation, but we still have discernible underestimation of surface O_3 in this region.

Although there are some discrepancies between simulated and observed surface O_3 as noted above, our model has reasonable ability to reproduce the absolute concentration and seasonal variation of surface O_3 in the Northern Hemisphere mid-latitudes, in particular in the East Asian region, which allows us to analyse the S-R relationship for O_3 in the East Asia.

3.3 Contributions to monthly mean East Asian surface O_3

Six-year averaged seasonal evolutions of monthly mean surface O_3 and the contributions from individual source regions in the PBL averaged within ten receptor areas within the East Asian region are shown in Fig. 4. We set the ten receptor areas as illustrated in the map in the middle of Fig. 4: East Japan (JPN-E), West Japan (JPN-W), North Japan (JPN-N), South Japan (JPN-S), North Korea (KOR-N), South Korea (KOR-S), Northeast China (CHN-NE), North China Plain (CHN-NCP), Yangtze

ACPD
10, 9077–9120, 2010

River Basin (CHN-YRB), and Southeast China (CHN-SE). These separations of receptor areas are mainly based on the climatic zone separations used in meteorological studies and statistics (e.g., Liu et al., 2005; Endo and Yasunari, 2006). The difference in the spatial distribution or temporal variation of meteorological features (e.g., temperature, precipitation, stream pattern) which define the climatic zone separations likely also affect the spatial distribution or temporal variation of air pollutants; thus it is expedient to employ these separations for receptor areas.

We can see some mutual features in the seasonal variations of surface O_3 over almost all receptor areas. Firstly, the contribution of the stratosphere contributes the largest proportion from the winter to early spring, and has a minimum in summer. The minimum of the stratospheric contribution in CHN-NE occurs later in autumn, similar to the case of the Eurasian continental sites (Mondy and Issyk Kul) depicted in Fig. 2. Secondly, there is a contribution of about 5–10 ppbv originating from the FT all year round with a small seasonal variation having a moderate peak from late summer to autumn. On the other hand, the contribution of the PBL shows different seasonal variation depending on the receptor area. It has a maxima in spring and autumn in the southern areas (CHN-YRB, CHN-SE, JPN-S), in summer in the northern continental areas (CHN-NCP and CHN-NE) and in spring over most of Japan and the Korean Peninsula.

In order to show the seasonal variation of the relative contribution of transported O_3 from outside of each receptor area, two red lines are superimposed on the upper plot of each figure. A solid line for each receptor area displays the ratio between the total O_3 mixing ratio and the sum of the mixing ratios of O_3 tracers assigned to all source regions except the PBL source region including that receptor area. For example, in the case of JPN-N, the sum of all O_3 tracers except that assigned to the PBL of Japan (JPN) divided by the total O_3 is shown as the red solid line. Note that for JPN-S, the exception from the summation is not JPN but ECS, because the receptor area of JPN-S is located inside the source region of ECS. Broken lines indicate a similar ratio but the sum is taken over the O_3 tracers which are assigned to the PBL of East Asian and adjacent

ACPD
10, 9077–9120, 2010

source regions (CHN, KOR, ECS, JPS, JPN, IDC, and ESB) except for the source region which includes the receptor area for that figure; e.g., JPN is excluded from the summation for JPN-N. In brief, the solid lines indicate the percentage of O_3 transported from all foreign source regions, and consequently the space between the solid line and the top transverse denotes the percentage of domestic pollution. The broken lines indicate the percentage of O_3 originating from the PBL of foreign source regions in East Asia. Strictly, they include the contributions from non-East Asian source regions (IDC, ESB), but we refer them as the East Asian contribution for the sake of clarity. Therefore, the difference between these two lines indicates the percentage of O_3 created outside the PBL of East Asian region, which includes the FT and stratosphere as well as distant source regions such as Europe or North America, and transported from there.

As shown in Fig. 4, contributions of O_3 transported from outside of the East Asian PBL becomes large in the cold season (October to March), and accounts for over 70% of the total O_3 in winter except in the southern part of China (CHN-YRB, CHN-SE). In the southern part of China, half of the total O_3 is chemically produced in the PBL of the CHN source region, i.e., domestic pollution, even in the winter, but in northeast China (CHN-NE), over 80% of total O_3 is transported from outside of East Asia and domestic pollution accounts for less than 10% in the same season. The largest part of O_3 originating from outside the East Asian PBL is attributable to the stratosphere and the second largest is the contribution from the FT in every receptor area. In addition to this, the contribution of distant PBL source regions, mainly composed of North America (AMN), Europe (EUR), North Atlantic Ocean (NAT), and Central Asia (CAS), becomes important in the cold season. The sum of these contributions can exceed 5 ppbv except for southern China, and can even be close to 10 ppbv in CHN-NE. Note that the contribution of EUR is largest in early spring (May) in most areas, whereas that of AMN is largest in winter. Such difference in seasonal dependencies of contribution is consistent with the previous estimation of the impact from European and North American emission sources on O_3 concentration in Japan using the emission sensitivity method (Wild and Akimoto, 2001; Wild et al., 2004). In winter, low temperatures and

ACPD
10, 9077–9120, 2010

weak Ultra-Violet (UV) radiation from the sun extends the chemical lifetime of O_3 so that O_3 created in distant source regions can survive the journey to East Asia. Furthermore, the Siberian High established over Eurasia in winter offers an efficient pathway to such O_3 from Europe to Asia (Wild et al., 2004).

In contrast, in the warm season (April to September), the contribution from domestic pollution and O_3 produced in foreign source regions in East Asia becomes large, while the influence from outside of the East Asian PBL decreases. The O_3 created in East Asia accounts for about half of the total O_3 in spring and up to about 70% in summer for areas other than in CHN-NE and JPN-S. During the warm season, strong UV radiation activates the photochemical reactions relevant to both the formation and destruction of O_3 in the atmosphere, so that vigorous chemical production of O_3 take place but its chemical lifetime also becomes short. This means that O_3 produced in distant regions is mostly lost before reaching the East Asian region, but a large amount of O_3 can be created inside the East Asian region and is subject to the short range transport such as intra-continental transport inside East Asia before it is chemically lost from the atmosphere.

The leading component of surface O_3 in each receptor area in the warm season is domestically-produced O_3, but the contribution second to this is different depending on the receptor area. In CHN-NE, there is a significant contribution from East Siberia (ESB), and the contribution from the Indochina Peninsula and the Philippines (IDC) is predominant in CHN-SE. Fairly large contributions from ESB and IDC also can be seen in JPN-N and JPN-S, respectively. In every receptor area in Japan and the Korean Peninsula, CHN provides the principal contribution after the domestic one, and the adjacent maritime PBL (NPC, JPS, and ECS) also provide large contributions. The precursors of these maritime O_3 would be originally emitted in the surrounding land area such as China, the Korean Peninsula, or Japan, since there are no large emitters in the ocean. In this sense, these maritime contributions should be apportioned to the emission sources on land. However, in the framework of the tagged tracer method, we can't attribute them to any particular emission source, because this

ACPD
10, 9077–9120, 2010

method is not aimed at estimating the overall impacts of the emission of O_3 precursors from any given region on local O_3, but evaluating the contributions of O_3 chemically produced in that region (Li et al., 2008). Therefore, we have to carefully interpret the results.

Figure 5 restructures a part of Fig. 4 to show the seasonally-averaged relative contributions from each source region for spring and summer, when the contributions of O_3 chemically produced inside East Asia are generally large. Several contributions that have common features are grouped: ASea (Adjacent Sea) is the sum of NPC, JPS and ECS; IDC+ is the sum of IDC and IND; and RMT (ReMoTe) is the sum of AMN, EUR, CAS, MES and NAT. The contributions of East Asian source regions including domestic pollution and that originating from outside of the East Asian PBL are comparable in spring, especially in central Japan (JPN-E+W), the Korean Peninsula (KOR), and CHN-NCP, while the former well exceeds the latter in the summer.

In every receptor area other than CHN-NE, domestic pollution is the principal contributor to the total O_3 in spring, which provides 20% in JPN-E+W and KOR, 40% in CHN-NCP, and almost half of total O_3 in the southern part of China (CHN-YRB, CHN-SE). In summer, the share of domestic pollution increases in every receptor area. The share is almost doubled from spring to summer in JPN-E+W, KOR, and CHN-NE, which makes the domestic contribution dominant, even in CHN-NE.

The springtime stratospheric contribution is around 20% in JPN-E+W and KOR, and shows an apparent dependence on latitude in China; its relative contribution increases from south (11% in CHN-SE) to north (27% in CHN-NE). A similar tendency is seen for the springtime relative contribution of RMT, but its contribution is somewhat lower than that from the stratosphere in all receptor regions. The relative contribution from RMT is 13% in JPN-E+W and KOR, and ranges from below 5% in CHN-SE to 21% in CHN-NE. The contributions from the stratosphere are almost halved in every receptor area in summer. Those from RMT undergo a greater reduction from spring to summer of over 50% in every receptor area. The relative contribution of the FT is generally larger in summer than in spring, but in some areas, part of this increase should be attributed

ACPD
10, 9077–9120, 2010

to the reduction of total O_3 from spring to summer, and the absolute contribution is nearly the same, as seen in Fig. 4.

The relative contribution of CHN upon KOR and JPN-E+W is similar in both seasons; around 20% and 10% in KOR and JPN-N+W, respectively. The Korean contribution to JPN-E+W is about 6% in spring, and less than 5% in summer. The combined relative contribution of CHN and KOR to JPN-E+W in spring, 17.8% as shown in Fig. 5, approximately corresponds to 10 ppbv, which is consistent with the previous estimation of regional O_3 build-up due to Chinese and Korean sources in spring around Japan (Tanimoto et al., 2005). Due to the dominance of westerly winds, westward transport of O_3 is limited in spring; consequently, the contribution of JPN to KOR or those from JPN and KOR to each receptor area in China are generally small in spring. In summer, the wind direction has no apparent preference for westerly winds as shown in Fig. 3; thus the westward transport of O_3 can occur somewhat more frequently than in spring. As a result, the contributions from JPN to KOR or KOR to CHN-NCP can account for 5% of total O_3 in summer. There are also relatively large contributions attributed to ASea, which would originate from the O_3 precursor emissions in CHN, KOR, or JPN, and thus should be attributed to those source regions. Therefore the contributions from East Asian source regions other than ASea presented in Figs. 4 and 5 and Table 2 should be considered as the minimum estimations of contributions for each source region.

The relative contribution from ESB is generally large in the northern areas. In CHN-NE, it account for about 10% and 12% of total O_3 in spring and summer, respectively. The contribution from ESB to CHN-NE peaks in May (≈8 ppbv) and remains almost constant of about 5 ppbv in summer, as seen in Fig. 4. In other areas, the relative contribution from ESB is generally larger in spring than in summer. In southern areas in East Asia, IDC and India (IND) provides significant contributions in the warm season. They share about 17% of total O_3 in CHN-SE and nearly 5% in CHN-YRB. In JPN-E+W, relative contributions both from ESB and IDC (+IND) account for at most 4% each even in the warm season. However, their contributions are quite large in JPN-N

ACPD
10, 9077–9120, 2010

and JPN-S; the relative contribution from ESB to JPN-N is about 7% in spring, and that from IDC (+IND) to JPN-S accounts for about 13% in summer.

The averaged contributions of source regions to each receptor area in spring and summer are summarized in Table 2. Table 2 shows the 6-year (2000–2005) averaged seasonal mean contributions and the coefficient of variation of the seasonal means during the six years rather than standard deviation. Because the seasonal mean for spring and summer can differ considerably, standard deviation is not a good indicator of interannual variation of seasonal means.

The relative interannual variations of the contributions from source regions in East Asia to Japan are generally larger in summer than in spring. This is likely due to the seasonal difference in the meteorological conditions around Japan which transport O_3 from the East Asian source regions to Japan.

The relative interannual variations in the contributions from RMT, FT, and STR to each receptor area in East Asia are generally smaller than those in the contributions from East Asian source regions. The coefficient of variations of the seasonal mean contributions from RMT, FT, and STR are lower than 15% for spring and summer, and also in autumn and winter (not shown). This demonstrates that regions outside of East Asia supply a steady amount of O_3 in each year to the East Asian region, which forms a baseline O_3 for East Asia.

3.4 One-hourly mean surface O_3 over Japan: validation and features

Since the current national Ambient Air Quality Standard (AAQS) for O_3 in Japan (60 ppbv) is provided by one-hourly mean concentration of O_3, special focus is placed on the one-hourly mean model output of surface O_3 hereinafter. Figure 6 compares the simulated and observed seasonal variation of the frequency distribution of one-hourly mean surface O_3 over Japan. Note that these frequencies are area-averaged; frequencies in each model grid are summed to calculate the total frequency in all model grids over Japan, then divided by the number of model grids to form the area-averaged frequency.

One-hourly surface O_3 data observed at ambient air quality monitoring stations from 2000 to 2005 compiled by the Atmospheric Environmental Observation System (AEORS) are used for comparison to the model results. About 1000 monitoring stations are widely distributed throughout Japan except in the southern islands. The monitoring data are averaged in each model grid over Japan, thus, extremely high or low O_3 values in the raw data are smoothed. Since the horizontal resolution of our model (≈200 km) is not fine enough to simulate the dissipation of O_3 at nighttime due to NO-titration in the ambient atmosphere, the model necessarily overestimates the nighttime O_3 mixing ratio in urban areas. Therefore, we select monitoring data obtained in daytime, from 10:00 to 16:00, in residential (not mid-urban or industrial) areas for appropriate comparison with the model results. Only daytime O_3 calculated by the model is used for the comparison.

The ridge line of the frequency distribution in the observation is high (40–50 ppbv) in spring and decreases to 20–30 ppbv in summer, which is consistent with the seasonal variation of monthly mean surface O_3 observed at Japanese monitoring sites shown in Fig. 2. The range of the frequency distribution extends toward higher concentrations in summer, thus the distribution is wider in summer than in spring. In summer, the ridge of the distribution is lowest, but the frequency of the occurrence of high surface O_3 mixing ratio, such as over 90 ppbv, also increases. As mentioned before, since Japan is largely affected by the intensified North Pacific High in summer, the frequency of observations of low concentrations of O_3 from clean maritime air is increased. However, with the most active photochemical productivity of O_3 also in summer, high concentrations of O_3 can also be produced if the meteorological conditions become so stable that the precursors of O_3 accumulate and fuel O_3 production in urban areas.

These observed features in the frequency distribution of one-hourly mean surface O_3 concentration are roughly simulated by the model; in particular, the seasonal transition of the ridge line of the distribution and the extension of the distribution to high concentrations in summer are consistent with the observation. However, it is apparent that the model cannot simulate the occurrence of high concentrations of O_3 over 100 ppbv in

summer and low concentrations less than 20 ppbv in non-summer seasons. This failure at lower O_3 concentrations is mainly a result of the inability of the model to simulate nighttime low O_3, as mentioned before, due to the coarse horizontal resolution of the model. The coarse horizontal resolution also results in the lack of high O_3 events in summer. Very dense accumulation of O_3 in urban areas cannot be resolved adequately by the 200 km grid spacing.

Although one-hourly model data are not suitable for the discussion of extremely high O_3 events in summer or nighttime low O_3, the intermediate range that accounts for most of the frequency distribution of O_3 can be reasonably simulated in the model. The well reproduced occurrence of one-hourly O_3 over 60 ppbv (Japan's AAQS of O_3) in the model makes the analysis of model data worthwhile. Thus, we further analyse one-hourly data below.

3.5 Contributions to one-hourly mean surface O_3

Figure 7 shows the one-hourly relative contributions from each source region in spring, calculated separately for four classes of one-hourly mean total O_3: low (0 to 30 ppbv), middle (30 to 60 ppbv), high (60 to 90 ppbv), and extra-high (over 90 ppbv) concentrations of O_3; for highly populated receptor regions in East Asia at a similar latitude. One-hourly relative contributions are calculated by dividing the one-hourly absolute contributions from each source by the one-hourly total O_3. The mean and 10, 25, 50, 75, and 90 percentiles over the whole 6-year period of calculation are shown in Fig. 7. The ranges from the 10 to 90 percentiles for several sources are fairly large, which often exceeds 30% for the leading sources in particular. This means that the one-hourly relative contributions from those source regions can vary considerably. In other words, the S-R relationship for O_3 can vary considerably hour by hour. However, because we intend to discuss the general features of the S-R relationship for O_3 in each O_3 class and also elucidate the differences between the O_3 classes, we describe the features and differences mainly based on the mean or median of one-hourly relative contributions hereinafter.

ACPD
10, 9077–9120, 2010

These plots should be compared to the upper plot of Fig. 5 that also shows the relative contributions from each source regions in spring but calculated using the monthly mean absolute contributions. For three areas shown in Fig. 7, this "mean" S-R relationship for O_3 depicted in Fig. 5 largely reflects that of the middle (30–60 ppbv) and high (60–90 ppbv) O_3 classes, while the S-R relationships for O_3 in the low (0–30 ppbv) and extra-high (>90 ppbv) O_3 classes are fairly different from the mean S-R relationship. The relative contribution from domestic pollution becomes more dominant in the higher O_3 classes. In the extra-high O_3 class, the relative contribution of domestic pollution roughly accounts for 50%, 50%, and 70% of total O_3 in JPN-E+W, KOR, and CHN-NCP, respectively. In the low O_3 class, domestic pollution is no longer the principal component of surface O_3 in every receptor area, instead large contributions originate from source regions that do not have leading contributions in the mean S-R relationship for O_3; the influences of ASea and FT become predominant in JPN-E+W, whereas ASea and JPN has greater contributions than in the mean S-R relationship in KOR. In CHN-NCP, the mean and median of the domestic contribution are overtaken by those of RMT or the stratosphere in the low O_3 class.

The S-R relationship for O_3 among the three main East Asian countries can vary according to the rank of O_3. The mean relative contribution from CHN to JPN-E+W is around 10% in every class of O_3 with the 10-90 percentile of relative contribution ranging from a couple of percents to about 20% (up to 30% in the high O_3 class). On the other hand, the relative contribution from KOR is almost negligible in the low O_3 class, but its range of distribution widens in the higher O_3 classes and the relative contribution occasionally exceeds 10% in the middle O_3 class and reaches almost 20% in high O_3 class. The contribution of CHN to KOR is large and comparable to that of domestic pollution in the low and middle O_3 classes. In the high O_3 class, CHN still has a large influence on KOR; the 10–90 percentile range of the relative contribution from CHN and that from domestic pollution overlap considerably. In the extra-high O_3 class, the contribution of CHN to KOR is generally larger than those to JPN-E+W. Since CHN-NCP is located upwind of Japan and the Korean Peninsula in spring, the influences of

ACPD
10, 9077–9120, 2010

those regions on CHN-NCP are generally small with an occasional large contribution of KOR in the middle and high O_3 classes. Therefore for CHN-NCP, the contribution of RMT, which includes central Asia (CAS) located upwind of China, is the second largest among the source regions in the PBL after the PBL of CHN.

The relative contribution of RMT to CHN-NCP gradually decreases as the class of O_3 increases, but the absolute contribution stays approximately constant at 6–8 ppbv in every O_3 class. Similarly, the absolute contributions of FT and STR are 5–8 ppbv and 9–11 ppbv, respectively. Note that the absolute contributions of RMT, FT, and STR to JPN-E+W and KOR are very similar to those to CHN-NCP except in the low O_3 class. The similarity among the absolute contributions of RMT, FT, and STR to these East Asian receptor areas is also seen in the other seasons. This demonstrates that such source regions outside of East Asia provide a baseline for O_3 in East Asia all year round.

Similar features of the relative contributions from each source region in each class of O_3 are evident in summer, although the respective values of the contributions are different; generally, the contribution of domestic pollution is intensified and those of STR and RMT decline in every O_3 class.

For the class of O_3 over 60 ppbv (Japan's AAQS), domestically-produced O_3 provides the principal contribution in both the high and extra-high O_3 classes to central Japan (JPN-E+W). Table 3 summarizes the mean absolute and relative contributions from each source region to central Japan in the high and extra-high O_3 classes in spring and summer. The domestic contribution is smaller in the high O_3 class than in the extra-high O_3 class in both seasons. In contrast, the relative contributions from foreign sources are generally greater in the high O_3 class than in the extra-high O_3 class, reflecting that the absolute contribution from each foreign source remains rather constant between both O_3 classes in each season. The approximate numbers of the absolute contribution from leading foreign sources are as follows: CHN (10 ppbv in spring, 8 ppbv in summer), KOR (5 ppbv, 6 ppbv), ASea (5 ppbv, 5 ppbv), RMT (6 ppbv, 2 ppbv), FT (7.5 ppbv, 7.5 ppbv), and STR (10 ppbv, 5 ppbv), respectively. These model

ACPD
10, 9077–9120, 2010

results suggest that the impact of foreign sources on the exceedance of Japan's AAQS is the most critical in the high O_3 class (60–90 ppbv) in spring. For the same O_3 class in summer, absolute contributions of East Asian foreign sources are nearly the same as in spring, and those from the intercontinental transport (RMT) and the stratosphere decrease relative to spring.

4 Summary and conclusions

In this study, we investigated the S-R relationship for O_3 in East Asia for the early 2000s through a multi-year simulation using the global chemical transport model CHASER with the tracer tagging method. The contributions of source regions of O_3 in the global atmosphere on surface O_3 in East Asia were quantitatively estimated with special focus on the role of intra-continental transport of O_3 within East Asia as well as the transport of O_3 from distant regions. The difference of the S-R relationship for O_3 in different classes of one-hourly O_3 concentration was also discussed.

Modelled surface O_3 was evaluated through comparison with the observations over an extensive longitudinal range in the Northern Hemisphere mid latitudes. The model well simulated several characteristic seasonal variations of surface O_3 such as the broad summer peak at inland mountainous areas and the spring peak and summer minimum at the maritime remote sites. Although there were some quantitative problems whose causes have not yet been identified at several sites, the model properly reproduced the regional difference in the seasonal transition of surface O_3 in East Asia.

Our simulation demonstrated the significant seasonal difference in the origin of surface O_3 in East Asia. O_3 transported from outside of the East Asian PBL with leading contributions from the stratosphere, free troposphere, Europe, North America, North Atlantic, and Central Asia accounted for the largest portion of surface O_3 (over 70%) in winter except for in southern China. In contrast, the share of O_3 created in East Asia reached 50% in spring, and further increased to around 70% in summer in most areas of East Asia. The main component of this O_3 was domestic in origin, which accounts

for over 20% and 40% of total O_3 in spring and summer, respectively, in most areas. The relative contribution of China to Japan and the Korean Peninsula was estimated to be about 10% and 20%, respectively, and the Korean contribution to Japan is around 5% in the warm season. The contribution from the East Siberia to Northeast China account for about 10%, and that from the Indochina Peninsula to Southeast China is about 17%. The relative contribution of intercontinental transport from distant sources in spring is the highest in Northeast China (21%) and about 13% in the Korean Peninsula and Japan. The interannual difference in this S-R relationship for O_3 was generally small for distant sources (<15%) but was sometimes large for East Asian sources particularly in summer.

Air quality monitoring data over Japan was analysed to demonstrate the seasonal variation of the frequency distribution of one-hourly mean surface O_3. The most frequently observed O_3 concentration was 40–50 ppbv in spring, which decreased to 20–30 ppbv in summer. The frequency of occurrence of high O_3 (over 90 ppbv) increased in summer, making the range of the frequency distribution wider in summer than in spring. The model roughly simulated these observed seasonal transitions in the frequency distribution.

We showed the difference in the S-R relationship for O_3 estimated separately according to the class of one-hourly total O_3 concentration in spring. In every O_3 class except the lowest (<30 ppbv), domestic pollution is the main contributor whose share increased in the higher O_3 classes; over 50% in extra-high O_3 class (>90 ppbv). The mean relative contribution to central Japan from China was about 10% in every class of O_3, but that from the Korean Peninsula became significant only in the middle and higher O_3 classes (>30 ppbv). China was estimated to have a large impact almost comparable to domestic pollution on the Korean Peninsula except in the extra-high O_3 class (>90 ppbv). In contrast, China has received relatively little impact from Japan or the Korean Peninsula in spring. Contributions from sources outside of the East Asian PBL including the stratosphere, free troposphere, Europe, North America, North Atlantic, and Central Asia contributed steady amounts of O_3 to East Asia in every O_3

class in each season, which constitutes the baseline O_3 in East Asia. The model results suggested that the impact of such foreign sources on the exceedance of Japan's AAQS is the most critical in the high O_3 class (60–90 ppbv) in spring.

Acknowledgements. This research was supported by the Global Environment Research Fund (C-081 and S-7) by the Ministry Of the Environment (MOE), Japan, and the Asian Environment Research Program at National Institute for Environmental Studies (NIES). We would like to acknowledge the entire staff of the EANET and the air quality monitoring stations of the MOE and of local governments for carrying out measurements and providing the observation. We thank the NOAA Earth System Research Laboratory, Global Monitoring Division; the German Meteorological Service, Hohenpeissenberg Meteorological Observatory; Instituto de Meteorologia, Portugal; Japan Meteorological Agency; National University of Ireland; Finnish Meteorological Institute; Environment Canada, Air Quality Research Branch; Federal Environmental Agency Germany; and Kyrgyz National University for providing ground based ozone data through the WDCGG data base. P. Pochanart is thanked for providing the surface O_3 data of Chinese mountain sites which was obtained through the GERF (B-051) by the MOE. The calculations were performed by NIES supercomputer system (NEC SX-8R). The GFD-DENNOU library was used for drawing the figures.

References

Akiyoshi, H., Zhou, L. B., Yamashita, Y., Sakamoto, K., Yoshiki, M., Nagashima, T., Takahashi, T., Kurokawa, J., Takigawa, M., and Imamura, T.: A CCM simulation of the breakup of the Antarctic polar vortex in the years 1980–2004 under the CCMVal scenarios, J. Geophys. Res., 114, D03103, doi:10.1029/2007JD009261, 2009.

Auvray, M. and Bey, I.: Long-range transport to Europe: Seasonal variations and implications for the European ozone budget, J. Geophys. Res., 110, D11303, doi:10.1029/2004JD005503, 2005.

Brasseur, G. P., Orlando, J. J., and Tyndall, G. S.: Atmospheric chemistry and global change, Topics in environmental chemistry, Oxford University Press, Oxford, New York, 1999.

Carmichael, G. R., Calori, G., Hayami, H., Uno, I., Cho, S. Y., Engardt, M., Kim, S. B., Ichikawa, Y., Ikeda, Y., Woo, J. H., Ueda, H., and Amann, M.: The MICS-Asia study: model inter-

comparison of long-range transport and sulfur deposition in East Asia, Atmos. Environ., 36, 175–199, 2002.
Chang, S.-C. and Lee, C. T.: Evaluation of the trend of air quality in Taipei, Taiwan from 1994 to 2003, Environ. Monit. Assess., 127, 87–96, 2007.
Chou, C. C.-K., Liu, S. C., Lin, C.-Y., Shiu, C.-J., and Chang, K.-H.: The trend of surface ozone in Taipei, Taiwan, and its causes: Implications for ozone control strategies, Atmos. Environ., 40, 3898–3908, 2006.
Derwent, R. G., Stevenson, D. S., Collins, W. J., and Johson, C. E.: Intercontinental transport and the origins of the ozone observed at surface sites in Europe, Atmos. Environ., 38, 1891–1901, 2004.
Emori, S., Nozawa, T., Numaguti, A., and Uno, I.: Importance of cumulus parameterization for precipitation simulation over East Asia in June, J. Meteorol. Soc. Jpn., 79, 939–947, 2001.
Endo, N. and Yasunari, T.: Changes in low cloudiness over China between 1971 and 1996, J. Climate, 19, 1204–1213, 2006.
Fiore, A. M., Jacob, D. J., Bey, I., Yantosca, Y. M., Field, B. D., Fusco, A. C., and Wilkinson, J. G.: Background ozone over the United States in summer: Origin, trend, and contribution to pollution episodes, J. Geophys. Res., 107(D15), 4275, doi:10.1029/2001JD000982, 2002.
Fiore, A. M., Dentener, F. J., Wild, O., Cuvelier, C., Schultz, M. G., Hess, P., Textor, C., Schulz, M., Doherty, R. M., Horowitz, L. W., MacKenzie, I. A., Sanderson, M. G., Shindell, D. T., Stevenson, D. S., Szopa, S., Van Dingenen, R., Zeng, G., Atherton, C., Bergmann, D., Bey, I., Carmichael, G., Collins, W. J., Duncan, B. N., Faluvegi, G., Folberth, G., Gauss, M., Gong, S., Hauglustaine, D., Holloway, T., Isaksen, I. S. A., Jacob, D. J., Jonson, J. E., Kaminski, J. W., Keating, T. J., Lupu, A., Marmer, E., Montanaro, V., Park, R. J., Pitari, G., Pringle, K. J., Pyle, J. A., Schroeder, S., Vivanco, M. G., Wind, P., Wojcik, G., Wu, S., and Zuber, A. : Multimodel estimates of intercontinental source-receptor relationships for ozone pollution, J. Geophys. Res., 114, D04301, doi:10.1029/2008JD010816, 2009.
Hayashida, S., Urita, N., Noguchi, K., Liu, X., and Chance, K.: Spatiotemporal Variation in Tropospheric Column Ozone over East Asia Observed by GOME and Ozonesondes, SOLA (Scientific online letters on the atmosphere), 4, 117–120, doi:10.2151/sola.2008-030, 2008.
Irie, H., Sudo, K., Akimoto, H., Richter, A., Burrows, J. P., Wagner, T., Wenig, M., Beirle, S., Kondo, Y., Sinyakov, V. P., and Goutail, F.: Evaluation of long-term tropospheric NO_2 data obtained by GOME over East Asia in 1996–2002, Geophys. Res. Lett., 32, L11810, doi:10.1029/2005GL022770, 2005.

Jacob, D. J., Logan, J. A., and Murti, P. P.: Effect of rising Asian emissions on surface ozone in the United States, Geophys. Res. Lett., 26(14), 2175–2178, 1999.

Kalnay, E., Kanamitsu, M., Kistler, R., Collins, W., Deaven, D., Gandin, L., Iredell, M., Saha, S., White, G., Woollen, J., Zhu, Y., Leetmaa, A., Reynolds, R., Chelliah, M., Ebisuzaki, W., Higgins, W., Janowiak, J., Mo, K. C., Ropelewski, C., Wang, J., Jenne, R., and Joseph, D. : The NCEP/NCAR 40-year reanalysis project, B. Am. Meteorol. Soc., 77, 437–470, 1996

Kanaya, Y., Pochanart, P., Liu, Y., Li, J., Tanimoto, H., Kato, S., Suthawaree, J., Inomata, S., Taketani, F., Okuzawa, K., Kawamura, K., Akimoto, H., and Wang, Z. F.: Rates and regimes of photochemical ozone production over Central East China in June 2006: a box model analysis using comprehensive measurements of ozone precursors, Atmos. Chem. Phys., 9, 7711–7723, 2009, http://www.atmos-chem-phys.net/9/7711/2009/.

Keating, T. J. and Zuber, A.: Hemispheric transport of air pollution 2007 interim report, Air Pollut. Stud. No. 16, U. N. Econ. Comm. for Europe, Geneva, 2007.

Kobayashi, K.: Assessing the impacts of tropospheric ozone on agricultural production, J. Jpn. Soc. Atmos. Environ., 34, 162–175, 1999.

Li, J., Wang, Z. F., Akimoto, H., Gao, C., Pochanart, P., and Wang, X.: Modeling study of the seasonal cycle of ozone in the boundary layer over East Asia, J. Geophys. Res., 112, D22S25, doi:10.1029/2006JD008209, 2007.

Li, J., Wang, Z., Akimoto, H., Yamaji, K., Takigawa, M., Pochanart, P., Liu, Y., Tanimoto, H., and Kanaya, Y.: Near-ground ozone source attributions and outflow in central eastern China during MTX2006, Atmos. Chem. Phys., 8, 7335–7351, 2008, http://www.atmos-chem-phys.net/8/7335/2008/.

Li, Q., Jacob, D. J., Bey, I., Palmer, P. I., Duncan, B. N., Field, B. D., Martin, R. V., Fiore, A. M., Yantosca, R. M., Parrish, D. D., Simmonds, P. G., and Oltmans, S. J.: Transatlantic transport of pollution and its effects on surface ozone in Europe and North America, J. Geophys. Res., 107(D13), 4166, doi:10.1029/2001JD001422, 2002.

Lin, M., Oki, T., Bengtsson, M., Kanae, S., Holloway, T., and Streets, D. G.: Long-range transport of acidifying substances in East Asia – Part II Source– receptor relationships, Atmos. Environ., 42, 5956–5967, 2008.

Lin, S.-J. and Rood, R. B.: Multidimensional flux-form semi-Lagrangian transport scheme, Mon. Weather Rev., 124, 2046–2070, 1996.

Liu, B., Xu, M., Henderson, M., and Qi, Y.: Observed trends of precipitation amount, frequency, and intensity in China, 1960–2000, J. Geophys. Res., 110, D08103, doi:10.1029/2004JD004864, 2005.
Lu, W.-Z. and Wang, X.-K.: Evolving trend and self-similarity of ozone pollution in central Hong Kong ambient during 1984–2002, Sci. Total Environ., 357, 160–168, 2006.
Ohara, T. and Sakata, T.: Long-term variation of photochemical oxidants over Japan, J. Jpn. Soc. Atmos. Environ., 38, 47–54, 2003.
Ohara, T., Akimoto, H., Kurokawa, J., Horii, N., Yamaji, K., Yan, X., and Hayasaka, T.: An Asian emission inventory of anthropogenic emission sources for the period 1980-2020, Atmos. Chem. Phys., 7, 4419–4444, 2007, http://www.atmos-chem-phys.net/7/4419/2007/.
Olivier, J. G. J. and Berdowski, J. J. M.: Global emissions sources and sinks, in: The Climate System, edited by: Berdowski, J., Guicherit, R., and Heij, B. J., A. A. Balkema Publishers/Swets & Zeitlinger Publishers, Lisse, The Netherlands, 33–78, 2001.
Pochanart, P., Kreasuwun, J., Sukasem, P., Geeratithadaniyom, W., Tabucanon, M. S., Hirokawa, J., Kajii, Y., and Akimoto, H.: Tropical tropospheric ozone observed in Thailand, Atmos. Environ., 35, 2657–2668, 2001.
Rayner, N. A., Parker, D. E., Horton, E. B., Folland, C. K., Alexander, L. V., Rowell, D. P., Kent, E. C., and Kaplan, A.: Global analyses of sea surface temperature, sea ice, and night marine air temperature since the late nineteenth century, J. Geophys. Res., 108(D14), 4407, doi:10.1029/2002JD002670, 2003.
Richter, A., Burrows, J. P., Nues, H., Grainer, C., and Niemeijer, U.: Increase in tropospheric nitrogen dioxide over China observed from space, Nature, 437, 129–132, 2005.
Roelofs, G.-J., Lelieveld, J., and van Dorland, R.: A three-dimensional chemistry/general circulation model simulation of anthropogenically derived ozone in the troposphere and its radiative climate forcing, J. Geophys. Res., 102(D19), 23389–23401, 1997.
Schultz, M. G., Heil, A., Hoelzemann, J. J., Spessa, A., Thonicke, K., Goldammer, J. G., Held, A. C., Pereira, J. M. C., and van het Bolscher, M.: Global wildland fire emissions from 1960 to 2000, Global Biogeochem. Cy., 22, GB2002, doi:10.1029/2007GB003031, 2008.
Stevenson, D. S., Dentener, F. J., Schultz, M. G., Ellingsen, K., van Noije, T. P. C., Wild, O., Zeng, G., Amann, M., Atherton, C. S., Bell, N., Bergmann, D. J., Bey, I., Butler, T., Cofala, J., Collins, W. J., Derwent, R. G., Doherty, R. M., Drevet, J., Eskes, H. J., Fiore, A. M., Gauss, M., Hauglustaine, D. A., Horowitz, L. W., Isaksen, I. S. A., Krol, M. C., Lamarque,

J.-F., Lawrence, M. G., Montanaro, V., Muller, J.-F., Pitari, G., Prather, M. J., Pyle, J. A., Rast, S., Rodriguez, J. M., Sanderson, M. G., Savage, N. H., Shindell, D. T., Strahan, S. E., Sudo, K., and Szopa, S.: Multimodel ensemble simulations of present-day and near-future tropospheric ozone, J. Geophys. Res., 111, D08301, doi:10.1029/2005JD006338, 2006.

Sudo, K., Takahashi, M., Kurokawa, J., and Akimoto, H.: CHASER: A global chemical model of the troposphere: 1. Model description, J. Geophys. Res., 107(D17), 4339, doi:10.1029/2001JD001113, 2002a.

Sudo, K., Takahashi, M., and Akimoto, H.: CHASER: A global chemical model of the troposphere: 2. Model results and evaluation, J. Geophys. Res., 107(D17), 4586, doi:10.1029/2001JD001114, 2002b.

Sudo, K. and Akimoto, H.: Global source attribution of tropospheric ozone: Long-range transport from various source regions, J. Geophys. Res., 112, D12302, doi:10.1029/2006JD007992, 2007.

Takigawa, M., Takahashi, M., and Akiyoshi, H.: Simulation of ozone and other chemical species using a Center for Climate System Research/National Institute for Environmental Studies atmospheric GCM with coupled stratospheric chemistry, J. Geophys. Res., 104, 14003–14018, 1999.

Tanimoto, H., Sawa, Y., Matsueda, H., Uno, I., Ohara, T., Yamaji, K., Kurokawa, J., and Tonemura, S.: Significant latitudinal gradient in the surface ozone spring maximum over East Asia, Geophys. Res. Lett., 32, L21805, doi:10.1029/2005GL023514, 2005.

Tanimoto, H.: Increase in springtime tropospheric ozone at a mountainous site in Japan for the period 1998–2006, Atmos. Environ., 43, 1358–1363, 2009.

US Environmental Protection Agency: Air Quality Criteria for Ozone and Related Photochemical Oxidants (Final), US Environmental Protection Agency, Washington, DC, EPA/600/R-05/004aF-cF, 2006.

van Leer, B.: Toward the ultimate conservative difference scheme, Part IV: A new approach to numerical convection, J. Comput. Phys., 23, 276–299, 1977.

von Kuhlmann, R., Lawrence, M. G., Crutzen, P. J., and Rasch, P. J.: A model for studies of tropospheric ozone and nonmethane hydrocarbons: Model descriptions and ozone results, J. Geophys. Res., 108(D9), 4294, doi:10.1029/2002JD002893, 2003.

Wang, H., Kiang, C. S., Xiaoyan, T., Xiuji, Z., and Chameides, W. L.: Surface ozone: A likely threat to crops in Yangtze delta of China, Atmos. Environ., 39, 3843–3850, 2005.

Wang, T., Wei, X. L., Ding, A. J., Poon, C. N., Lam, K. S., Li, Y. S., Chan, L. Y., and Anson, M.: Increasing surface ozone concentrations in the background atmosphere of Southern China, 1994-2007, Atmos. Chem. Phys., 9, 6217–6227, 2009, http://www.atmos-chem-phys.net/9/6217/2009/.

Wang, Y., Jacob, D. J., and Logan, J. A.: Global simulation of tropospheric O_3-NO_x-hydrocarbon chemistry: 3. Origin of tropospheric ozone and effects of nonmethane hydrocarbons, J. Geophys. Res., 103(D9), 10757–10767, 1998.

Wesely, M. L.: Parameterixstion of surface resistance to gaseous dry deposition in regional-scale numerical models, Atmos. Environ., 23, 1293–1304, 1989.

Wild, O. and Akimoto, H.: Intercontinental transport of ozone and its precursors in a three-dimensional global CTM, J. Geophys. Res., 106(D21), 27729–27744, 2001.

Wild, O., Pochanart, P., and Akimoto, H.: Trans-Eurasian transport of ozone and its precursors, J. Geophys. Res., 109, D11302, doi:10.1029/2003JD004501, 2004.

Wild, O.: Modelling the global tropospheric ozone budget: exploring the variability in current models, Atmos. Chem. Phys., 7, 2643–2660, 2007, http://www.atmos-chem-phys.net/7/2643/2007/.

Xu, X., Lin, W., Wang, T., Yan, P., Tang, J., Meng, Z., and Wang, Y.: Long-term trend of surface ozone at a regional background station in eastern China 1991-2006: enhanced variability, Atmos. Chem. Phys., 8, 2595–2607, 2008, http://www.atmos-chem-phys.net/8/2595/2008/.

Table 1. Statistical summary of the comparison between observed and modelled surface O_3 at observational sites shown in Fig. 2[a].

Station Name	Mean (Obs) [ppbv]	Mean (Model) [ppbv]	*R*	MB [ppbv]	RMSE [ppbv]
Mace-Head	37.81	33.57	0.73	−4.24	5.32
Pallas-Sammaltunturi	33.02	30.70	0.77	−2.32	4.16
Mondy	43.50	40.82	0.83	−2.68	4.44
Experimental-Lakes-Area	31.89	30.06	0.93	−1.82	2.98
Heimaey	39.75	28.43	0.88	−11.32	11.52
Hohenpreissenberg	41.05	45.59	0.93	4.54	6.99
Zugspitze-Schneefernerhaus	49.81	50.08	0.97	0.27	1.61
Issyk-Kul	39.54	40.46	0.91	0.92	2.22
Trinidad-Head	30.92	30.69	0.72	−0.23	3.44
Niwot-Ridge-Saddle	52.76	52.14	0.92	−0.62	2.07
Angra-do-Heroismo	29.49	34.78	0.88	5.29	6.37
Tudor-Hill	39.54	36.51	0.98	−3.03	4.02
Mauna-Loa	40.15	45.35	0.94	5.19	5.46
Rishiri	41.33	36.31	0.80	−5.02	7.25
Oki	43.00	45.69	0.82	2.69	5.21
Happo	55.58	47.18	0.95	−8.40	8.99
Ryori	39.06	41.77	0.92	2.71	3.77
Mt. Hua	50.29	57.46	0.91	7.18	8.25
Mt. Huang	47.23	51.95	0.79	4.72	7.25
Mt. Tai	56.18	57.34	0.93	1.17	4.52
Kanghwa	41.33	48.05	0.89	6.72	7.92
Cheju	36.75	45.95	0.94	9.20	9.54
Hedo	38.42	38.58	0.98	0.17	4.51
Ogasawara	28.08	30.74	0.97	2.66	4.00
Srinakarin	27.35	36.53	0.91	9.18	11.03

[a] All statistics are calculated by use of multi-year averaged monthly means shown in Fig. 2.

ACPD
10, 9077–9120, 2010

Table 2. Contributions (ppbv) from source regions to receptor areas in East Asia averaged in spring (March-April-May) and summer (June-July-August)[a,b].

			Receptor area																			
			JPN								KOR				CHN							
			N		E		W		S		N		S		NE		NCP		YRB		SE	
Source region	MAM	JPN	5.4	(12.4)	12.0	(3.7)	10.1	(6.6)	1.8	(25.0)	1.0	(37.9)	2.8	(34.3)	0.4	(25.9)	0.4	(26.5)	0.4	(46.3)	0.2	(51.6)
		CHN	3.8	(13.2)	5.3	(18.4)	7.1	(15.4)	6.3	(10.4)	11.1	(16.1)	9.9	(20.0)	6.8	(3.8)	20.9	(10.8)	32.0	(5.8)	23.3	(6.4)
		KOR	1.6	(18.7)	2.5	(15.5)	3.5	(8.8)	1.1	(16.2)	12.8	(6.3)	11.3	(7.2)	0.6	(5.6)	1.9	(24.8)	0.8	(35.0)	0.2	(33.6)
		Asea	4.2	(8.7)	4.1	(5.8)	5.1	(7.5)	8.8	(6.6)	2.2	(12.3)	3.9	(8.6)	1.5	(14.8)	1.1	(7.8)	1.3	(11.5)	1.4	(17.6)
		ESB	3.0	(12.0)	1.4	(12.9)	0.9	(14.2)	0.4	(18.6)	1.5	(10.6)	1.1	(13.9)	4.3	(9.2)	1.1	(14.1)	0.3	(24.4)	0.1	(33.9)
		IDC+	0.3	(7.6)	0.4	(6.0)	0.7	(7.9)	2.1	(20.0)	0.3	(7.9)	0.4	(5.3)	0.3	(12.0)	0.4	(14.9)	2.3	(21.8)	8.2	(9.7)
		RMT	7.0	(3.5)	6.7	(3.6)	6.4	(10.1)	4.3	(10.5)	7.0	(4.3)	6.7	(7.0)	8.8	(2.8)	7.5	(8.3)	4.4	(13.5)	2.1	(14.0)
		MISC	1.3	(11.1)	1.0	(7.4)	0.9	(6.4)	0.9	(5.4)	1.1	(6.5)	1.0	(5.7)	1.9	(5.5)	1.0	(7.6)	0.8	(5.5)	0.8	(10.9)
		FT	5.4	(4.3)	6.3	(2.9)	6.7	(5.3)	7.7	(4.7)	5.8	(3.4)	5.9	(4.8)	6.1	(3.3)	6.6	(5.5)	6.3	(5.1)	6.9	(5.4)
		STR	10.2	(8.4)	10.9	(10.3)	10.9	(8.5)	9.2	(6.3)	10.2	(9.4)	10.3	(10.0)	11.1	(8.5)	11.0	(9.5)	8.2	(9.6)	5.2	(7.8)
		TOTL	42.1	(4.5)	50.7	(2.0)	52.3	(2.9)	42.6	(3.6)	53.0	(3.5)	53.4	(3.0)	41.8	(1.6)	52.0	(2.9)	56.8	(3.3)	48.3	(4.4)
	JJA	JPN	10.6	(11.6)	19.8	(7.0)	14.0	(12.9)	1.0	(53.3)	1.4	(13.1)	4.1	(14.6)	0.6	(30.4)	0.3	(15.8)	0.4	(62.1)	0.2	(80.8)
		CHN	3.2	(22.0)	3.9	(28.7)	4.3	(28.4)	2.2	(27.1)	12.6	(16.6)	8.4	(18.6)	14.2	(6.5)	37.9	(7.6)	38.0	(7.7)	21.8	(10.0)
		KOR	2.0	(25.5)	1.8	(19.3)	1.7	(22.1)	0.2	(64.3)	21.7	(4.4)	16.8	(9.5)	1.2	(17.4)	3.2	(10.9)	0.7	(42.9)	0.1	(92.7)
		Asea	5.8	(8.3)	3.9	(8.0)	5.1	(5.2)	6.8	(9.1)	2.7	(11.0)	4.9	(6.8)	1.1	(26.2)	0.7	(14.7)	0.9	(29.8)	0.6	(44.8)
		ESB	1.7	(30.3)	0.4	(32.2)	0.2	(36.9)	0.0	(55.8)	0.9	(28.3)	0.5	(22.5)	4.8	(10.0)	0.9	(15.4)	0.2	(16.9)	0.0	(43.0)
		IDC+	0.3	(24.8)	1.0	(15.1)	1.6	(20.6)	3.3	(12.3)	0.6	(25.0)	1.2	(19.3)	0.1	(9.4)	0.5	(16.7)	2.3	(23.7)	6.7	(19.6)
		RMT	1.3	(12.7)	1.1	(6.4)	0.9	(10.7)	0.6	(14.7)	1.9	(9.1)	1.3	(13.4)	3.4	(6.8)	3.0	(4.2)	1.2	(12.2)	0.9	(11.3)
		MISC	0.8	(19.7)	0.6	(15.4)	0.7	(8.2)	1.0	(11.9)	0.7	(12.2)	0.7	(9.2)	1.6	(15.6)	0.8	(11.7)	0.7	(10.9)	1.1	(17.2)
		FT	4.8	(6.6)	6.8	(4.3)	7.5	(6.7)	8.8	(6.1)	7.1	(8.2)	6.8	(6.1)	8.1	(7.4)	8.7	(5.6)	7.4	(2.4)	8.0	(4.1)
		STR	2.6	(9.5)	2.5	(3.4)	2.2	(7.7)	1.7	(7.9)	4.0	(7.1)	2.7	(7.6)	6.0	(4.8)	5.7	(4.9)	2.4	(9.2)	1.5	(13.4)
		TOTL	33.4	(3.8)	41.9	(5.3)	38.3	(1.7)	25.5	(3.9)	53.6	(5.0)	47.4	(5.0)	41.0	(3.6)	61.7	(5.1)	54.0	(6.1)	40.9	(5.8)

[a] All contributions are averaged for 6 years.

[b] Values in brackets are coefficient of variation (in %), i.e., standard deviation among annual contributions divided by the 6-year averaged contribution and multiplied by 100.

Table 3. Mean one-hourly contributions from source regions to central Japan (JPN-E+W) in high O_3 (60–90 ppbv) and extra-high O_3 (over 90 ppbv) classes for spring (MAM) and summer (JJA)[a,b].

Regions	Mean contribution from source regions to central Japan, ppbv (%)			
	MAM		JJA	
	60–90	>90	60–90	>90
JPN	19.8 (29.0)	47.4 (50.8)	34.6 (50.5)	55.9 (59.8)
CHN	9.1 (13.6)	11.0 (11.8)	7.6 (11.1)	8.9 (9.6)
KOR	5.1 (7.6)	5.2 (5.6)	5.1 (7.4)	7.1 (7.6)
Asea	5.2 (7.7)	4.6 (4.9)	5.4 (8.0)	4.7 (5.1)
ESB	1.5 (2.2)	1.9 (2.1)	0.8 (1.1)	1.0 (1.0)
IDC+	0.5 (0.7)	0.2 (0.2)	0.8 (1.3)	0.4 (0.5)
RMT	6.8 (10.3)	5.3 (5.7)	1.8 (2.7)	2.2 (2.4)
MISC	1.1 (1.7)	1.0 (1.1)	0.7 (1.1)	0.6 (0.7)
FT	7.2 (10.8)	7.5 (8.1)	7.5 (11.1)	7.6 (8.1)
STR	10.8 (16.4)	9.1 (9.8)	4.0 (5.8)	5.0 (5.3)

[a] Values are shown in ppbv.
[b] Values in brackets denote relative contributions shown in %.

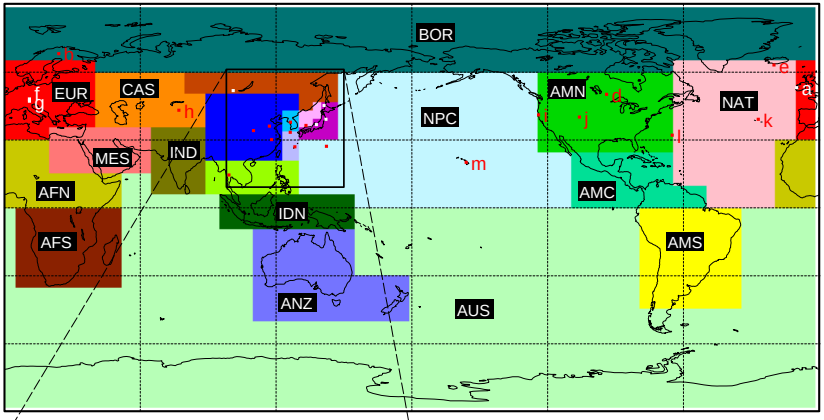

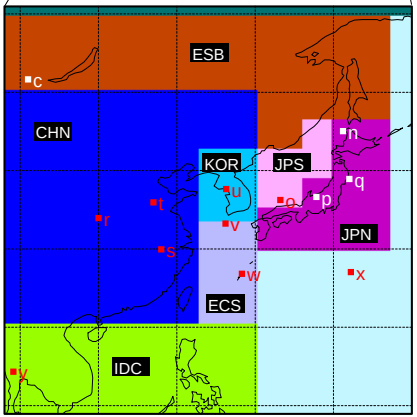

AMN : North America
AMC : Central America
AMS : South America
AFN : North Africa
AFS : South Africa
EUR : Europe
CAS : Central Asia
MES : Middle East
IND : India etc.
CHN : China etc.
KOR : Korean Peninsula
ECS : East China sea
JPS : Sea of Japan
JPN : Japan
IDC : Indochina, Thailand, and Philippines
IDN : Indonesia etc.
ANZ : Australia and New Zealand
ESB : East Siberia
NPC : North Pacific Ocean
NAT : North Atrantic Ocean
BOR : Arctic and subarctic region
AUS : Oceans in the S.H. and Antarctica

Fig. 1. Horizontal definition of source regions used to tag O_3 tracers. This horizontal separation is applied for both the PBL and FT. The East Asian region is expanded for clarity. Marked solid squares and letters next to them indicate the locations where the comparisons between observations and model calculations are shown in Fig. 2.

ACPD
10, 9077–9120, 2010

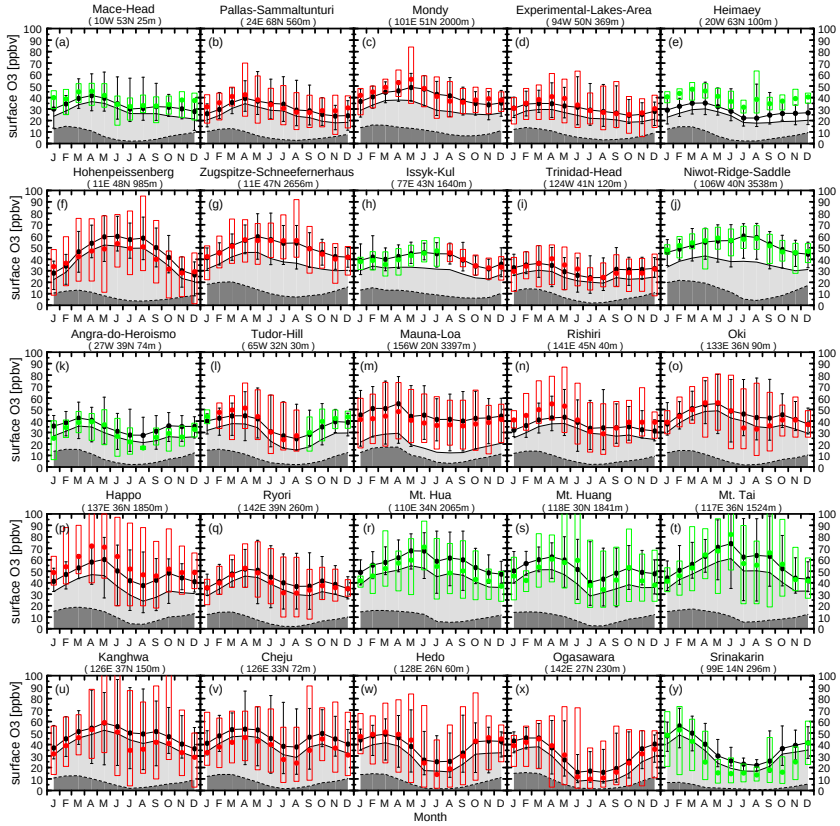

Fig. 2. Seasonal variations of monthly mean surface O_3 observations (red/green filled circles) and model calculations (black circles and black thick solid lines), with contributions from the stratosphere (dark gray), PBL (light gray), and FT (white) calculated by the model. Monthly means and each contribution are multi-year (6 years for model and available years for observation) averaged values. Vertical bars and boxes denote the multi-year range of daily mean surface O_3 in each month for model and observation, respectively. For observations, red (green) circles and boxes are for observational sites where more than (not exceeding) 2 years of data are available. Model calculations are interpolated to the longitude, latitude, and altitude of the location of each site.

ACPD
10, 9077–9120, 2010

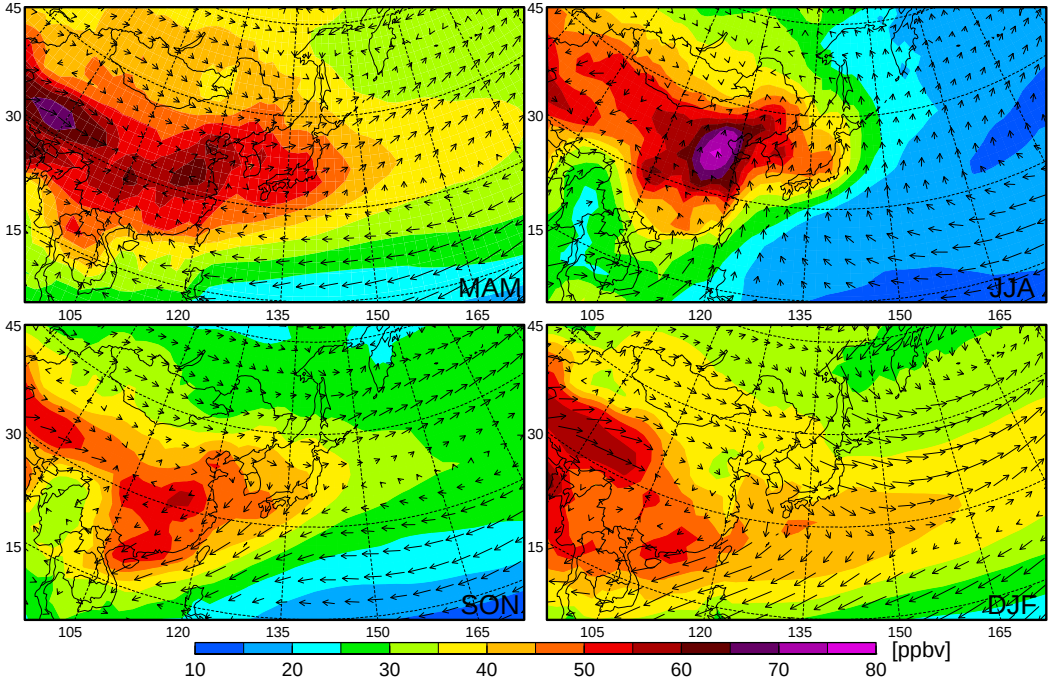

Fig. 3. Simulated seasonal mean surface O_3 (ppbv, colours) and wind vectors (m/s, arrows) in East Asia averaged for the 6 years of the calculation period.

ACPD
10, 9077–9120, 2010

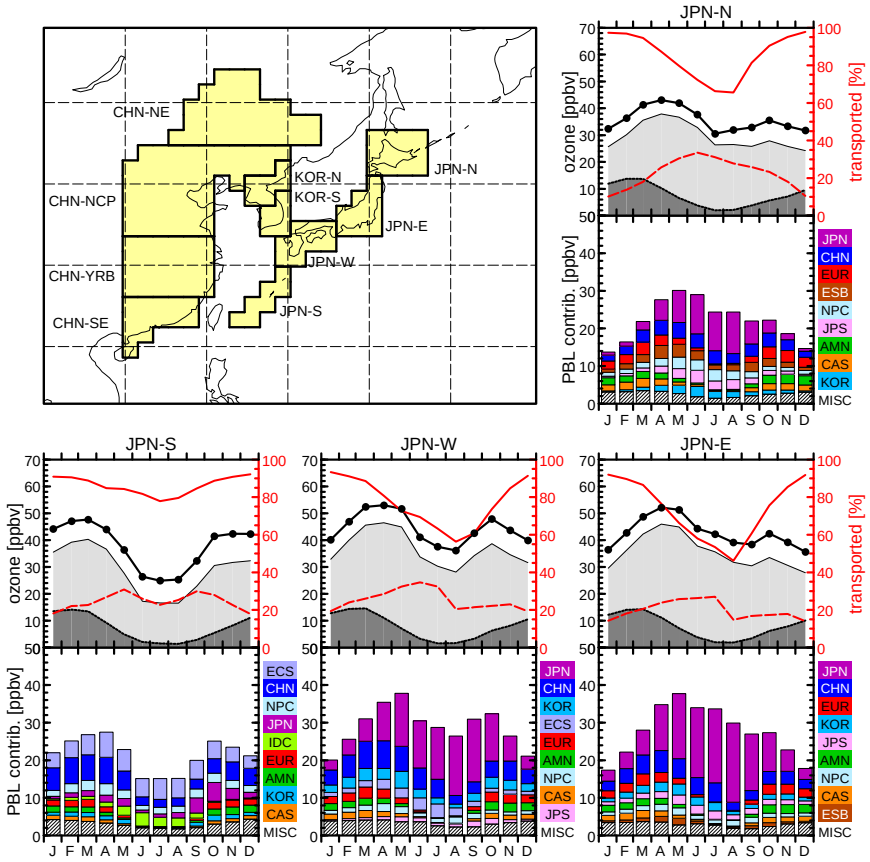

Fig. 4. (Top plots of each figure) Seasonal variations of area-averaged monthly mean surface O_3 with contributions from the stratosphere (dark gray), PBL (light gray), and FT (white) calculated by the model; areas of averaging are shown in the map. Red solid lines indicate the contribution (%) of O_3 transported from all foreign source regions and broken lines from foreign source regions in East Asia (see details in the manuscript). (Bottom plots of each figure) Contributions (ppbv) from the top nine source regions in the PBL and the sum of the rest of the PBL (MISC) are shown as stacked bar charts. Coloured boxes with the region names are stacked from top to bottom in order of annual mean contribution. All values are averaged for 6 years.

ACPD
10, 9077–9120, 2010

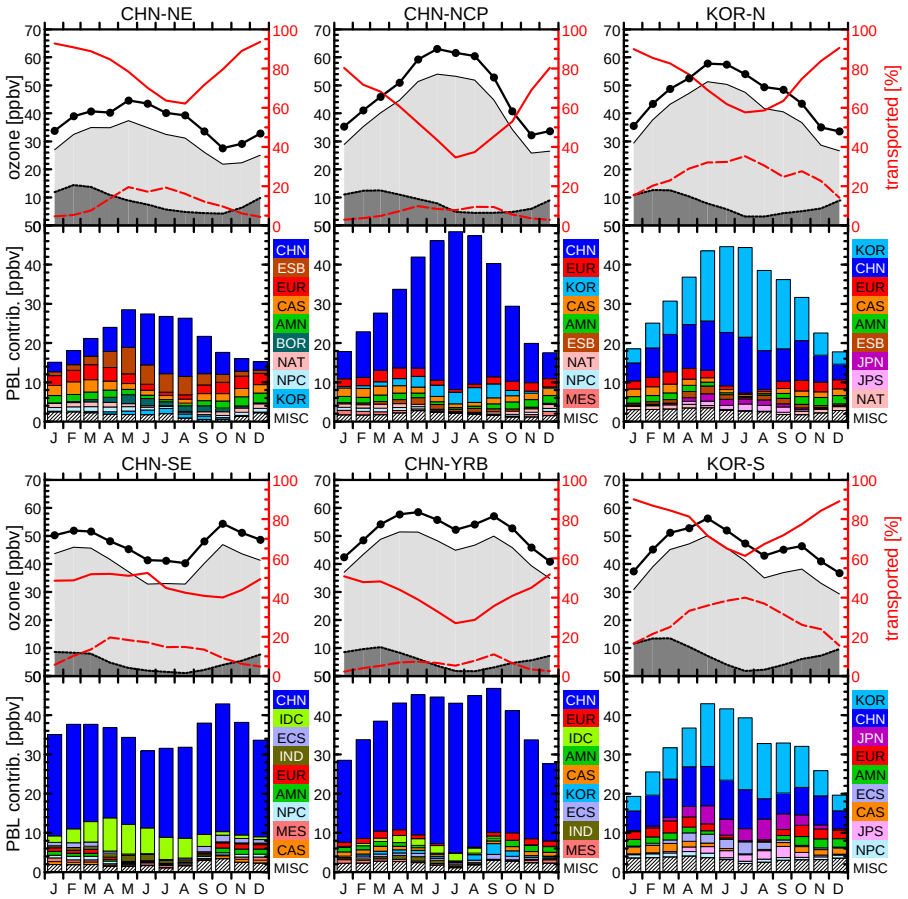

Fig. 4. Continued.

ACPD
10, 9077–9120, 2010

Importance of various source regions on East Asian surface ozone

T. Nagashima et al.

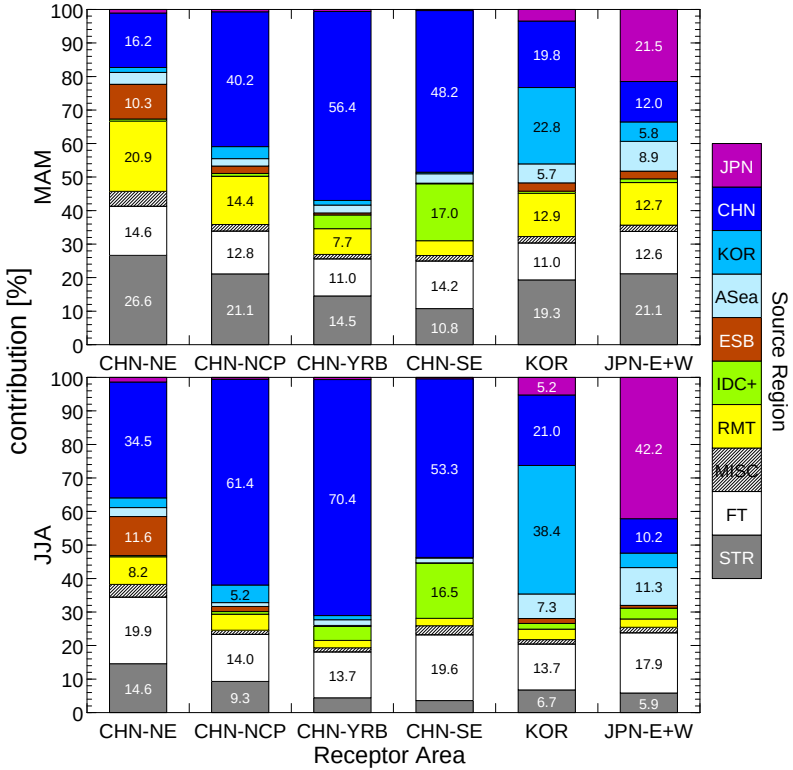

Fig. 5. Seasonal mean relative contribution (%) from source regions to receptor areas in East Asia for spring (top) and summer (bottom). Values are calculated by dividing seasonal mean contribution (ppbv) from each source region by seasonal mean total O_3 for each year and averaging for 6 years. Contributions greater than 5% are shown on the bar charts. For the source regions: ASea (Adjacent Sea) is the sum of NPC, JPS and ECS; IDC+ is the sum of IDC and IND, and RMT is the sum of AMN, EUR, CAS, MES and NAT. For receptor area; JPN-E+W is the sum of JPN-E and JPN-W, and KOR is the sum of KOR-N and KOR-S.

ACPD
10, 9077–9120, 2010

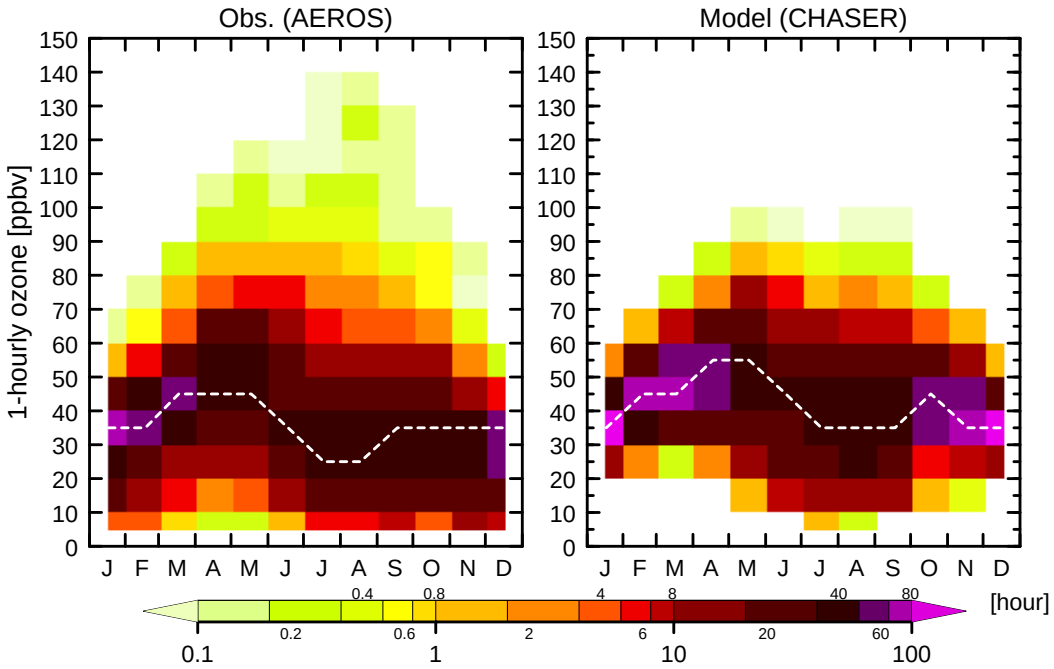

Fig. 6. Seasonal variations of the frequency distributions of daytime (10:00–16:00) one-hourly surface O_3 over Japan calculated by use of observations from the Atmospheric Environmental Regional Observation System (AEROS) (left) and model calculations (right). White dotted lines denote the ridge lines of frequency distributions. Frequency distributions are calculated for each year and then averaged to be shown as 6-year means.

ACPD
10, 9077–9120, 2010

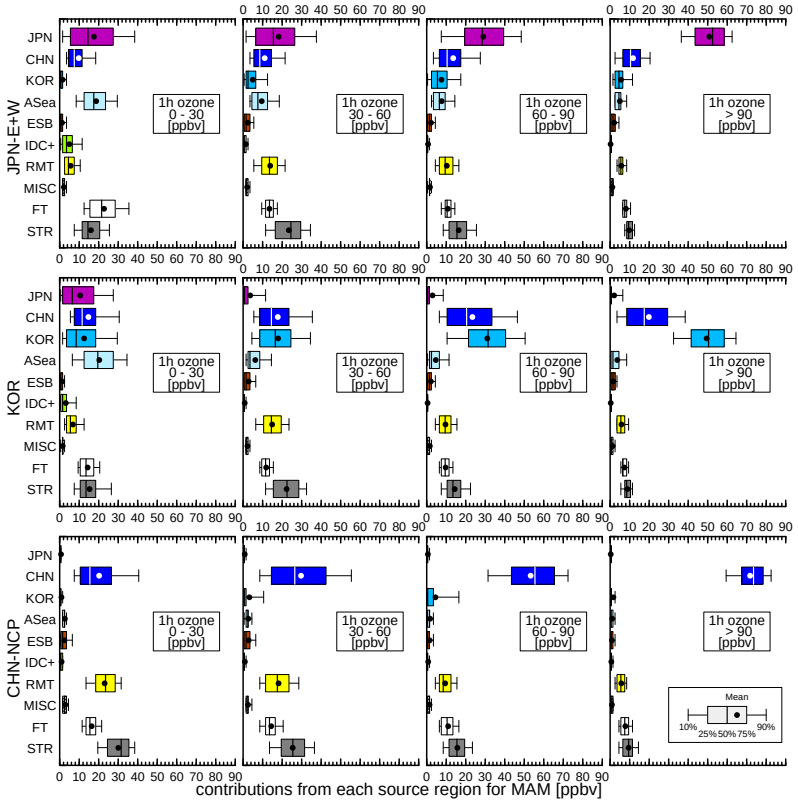

Fig. 7. One-hourly relative contribution (%) to total O_3 from source regions to central Japan (top), the Korean Peninsula (middle), and North China plain (bottom) for spring (MAM). The box-and-whisker plot represents the 10, 25, 50, 75, and 90 percentiles of one-hourly relative contribution from each source region in the whole 6-year period of calculation and the black filled circle shows the mean of one-hourly relative contribution in the period. All statistics are separately computed for four different classes of total O_3; low (0 to 30 ppbv), middle (30 to 60 ppbv), high (60 to 90 ppbv), and extra-high (over 90 ppbv) O_3.

ACPD
10, 9077–9120, 2010